GPS Velocity Field of the Western United States for the 2023 National Seismic Hazard Model Update

Yuehua Zeng[*1]

Abstract

Global Positioning System (GPS) velocity solutions of the western United States (WUS) are compiled from several sources of field networks and data processing centers for the 2023 U.S. Geological Survey National Seismic Hazard Model (NSHM). These solutions include both survey and continuous-mode GPS velocity measurements. I follow the data processing procedure of Parsons et al. (2013) for the Uniform California Earthquake Rupture Forecast, version 3 and McCaffrey, Bird, et al. (2013) and Zeng and Shen (2013) for their WUS deformation models in support of the 2014 NSHM update. All GPS velocity vectors are first rotated to a common North American reference frame. I edit the velocities to remove outliers and data with significant influence from volcanism. The solutions are then combined into a final GPS velocity field consisting of 4979 horizontal velocity vectors. I compute strain rates based on these GPS velocities using the method of Shen et al. (2015). These strain rates correlate closely with seismicity rates in the WUS. The results are used for WUS geodetic and geologic deformation modeling in support of the 2023 NSHM update.

Introduction

Modern Global Positioning System (GPS) velocities record contemporary surface deformation across the western United States (WUS) since late 1980s. These GPS observations measure ground motions with submillimeter per year precision and are often more robust and precise than data obtained from geologic studies. For the first time, the 2014 U.S. Geological Survey (USGS) National Seismic Hazard Model (NSHM) update (Petersen et al., 2014) incorporated GPS measurements directly into its models for seismic hazard assessment. A common set of GPS velocity data (McCaffrey, Bird, et al., 2013) was assembled at the time for crustal deformation modeling in support of the NSHM project (Petersen et al., 2013).

This article focuses on the GPS velocity field update. GPS solutions are first collected from all available sources of field networks and data processing centers. Following the same data processing procedure of Parsons et al. (2013) for Uniform California Earthquake Rupture Forecast, version 3 (UCERF3) and McCaffrey, Bird, et al. (2013) and Zeng and Shen (2013) for their 2014 WUS deformation models, these solutions are rotated to a common North American reference frame and vetted to remove outliers. The solutions are then combined into a final GPS velocity field. Based on these velocities, I compute strain rates and discuss their relation to seismic hazard considering their correlation with seismicity distribution across the WUS.

GPS Data and Processing

GPS velocity solutions are compiled from seven sources. Table 1 lists the origins of these sources. Most of these data sources cover the entire WUS. The Pacific Northwest data (McCaffrey and King, 2017) do not cover southern California. The University of California San Diego (UCSD) Scripps Institute of Oceanography campaign data (González-Ortega et al., 2018) cover only the northern Baja California. Studies have shown the importance of using vertical velocities to constrain earth uplift in regional deformation models (i.e., Hammond et al., 2018). Vertical velocities also provide critical constraint to the locking pattern along the Cascadia subduction plate (i.e., McCaffrey, King, et al., 2013). Errors in vertical GPS data, however, tend to be high for the maximum error criterion of 2 mm/yr that is applied to the

1. U.S. Geological Survey, Geological Hazard Science Center, Denver, Colorado, U.S.A., https://orcid.org/0000-0003-1161-1264 (YZ)

*Corresponding author: zeng@usgs.gov

TABLE 1
Regional GPS Network Data Processing History

Project/Program/Region	Network Type	Processing Institution	Reference
PBO	CGPS	CWU and MIT	Herring et al. (2016)
NGL/MIDAS	CGPS	NGL/UNR	Blewitt et al. (2016, 2018)
Pacific Northwest	CGPS and Survey	PSU and MIT	McCaffrey and King (2017)
Northern Baja California	Survey	Scripps, UCSD	González-Ortega et al. (2018)
WUS	CGPS and Survey	UCLA	Shen (2017)
MEaSUREs/WUS	CGPS	JPL and SOPAC	Bock et al. (2021)
WUS	CGPS and Survey	USGS	Murray and Svarc (2017)

CGPS, continuous mode GPS; CWU, Central Washington University; MIDAS, Median Interannual Difference Adjusted for Skewness; MIT, Massachusetts Institute of Technology; NGL, Nevada Geodetic Laboratory; PBO, Plate Boundary Observatory; PSU, Portland State University; SOPAC, Scripps Orbit and Permanent Array Center; UCSD, University of California San Diego; UCLA, University of California Los Angeles; UNR, University of Nevada Reno; USGS, U.S. Geological Survey; WUS, western United States.

horizontal velocities. In addition, nontectonic deformations recorded by the vertical data could further complicate the modeling of fault-slip rates in the WUS (Argus et al., 2014). For these and various other considerations for consistency, we decide to follow previous data processing procedures (McCaffrey, Bird, et al., 2013; Petersen et al., 2013) to consider horizontal velocities only for the current deformation modeling in support of NSHM.

The Geodesy Advancing Geosciences and EarthScope (GAGE) Facility GPS Data Analysis Centers produce position time series and velocities for about 2000 continuous-mode GPS (CGPS) operating stations around North America and the surrounding area (Herring et al., 2016). The Plate Boundary Observatory (PBO) is a part of this GAGE operation with 1100 CGPS stations. The final product is assembled at Massachusetts Institute of Technology (MIT) by merging two independent GPS solutions. One is a point-positioning based solution produced using the National Aeronautics and Space Administration (NASA) Jet Propulsion Laboratory (JPL) GIPSY/OASIS software at Central Washington University (CWU). The other is a network-based double-differencing product produced using the GAMIT software (Herring et al., 2015) at the New Mexico Institute of Mining and Technology. After removing coseismic and postseismic responses, seasonal variations, and other transient signals, GAGE analysis generates combined positioning time series and secular velocity relative to the North American reference frame NAM14. I acquire the WUS PBO combined velocity product from the UNAVCO Data Center in March 2020 (see Data and Resources), which is the last released version of the PBO products. These PBO products are part of the 2018 GAGE project and are no longer updated; only CWU products are processed and updated as part of the current GAGE project.

Developed at the Nevada Geodetic Laboratory (NGL), the Median Interannual Difference Adjusted for Skewness (MIDAS) algorithm is a robust GPS time-series trend estimator. After GPS time series are produced by NGL using the GIPSY software, MIDAS is applied to produce GPS velocities for CGPS stations around the globe. The MIDAS velocity product successfully removes data outliers, steps (i.e., coseismic offsets), and seasonal signals (Blewitt et al., 2016). The MIDAS velocity product for the WUS is obtained from the NGL website. Their velocity field includes solutions from semicontinuously operating stations operated by NGL, called the MAGNET GPS network. This network provides dense station coverage along the Walker Lane and most of western Nevada. Its data product is crucial for resolving fault-slip rates and crustal deformation west of the Basin and Range province. Although the postseismic signals are not specifically removed, velocities from MIDAS do not show significant biases in amplitude and azimuthal direction due to postseismic deformations from large California earthquakes. Examples are the 2010 **M** 7.2 El Mayor–Cucapah earthquake and the 1992 **M** 7.3 Landers and 1999 **M** 7.1 Hector Mine earthquakes, when I compare velocities from MIDAS to other GPS velocity products (i.e., the PBO and University of California Los Angeles [UCLA] solutions) in these earthquake source areas. Any differences between MIDAS and other velocity fields are attributed to the uncertainties in the final combined velocity solution.

The Pacific Northwest GPS velocities are provided by Robert McCaffrey (Portland State University [PSU], written comm., 2020). He and his team have collected new survey data from 71 sites up to 2016 and processed them together with continuous data from the PBO and The Pacific Northwest Geodetic Array (PANGA) networks (McCaffrey and King, 2017). These data were then combined with data from USGS and National Geodetic Survey data acquired since 1994 (McCaffrey and King, 2017). The data processing is done with the GAMIT and GLOBK software (Herring et al., 2018a) following the same processing procedures of McCaffrey et al. (2007).

The UCLA velocity data were made available to us by Zheng-Kang Shen (UCLA, written comm., 2020). This product is an update of the velocity field provided for the 2014 NSHM deformation modeling effort (McCaffrey, Bird, et al., 2013). Shen and his team first processed all the survey mode data archived in UNAVCO for the WUS region using the GAMIT software (Herring et al., 2018b) to obtain daily solutions. These daily solutions are then combined with the Scripps Orbit and Permanent Array Center (SOPAC; see Data and Resources) daily solutions of continuous GPS observations using the GLOBK software (Herring et al., 2015). The loosely constrained daily solutions are aggregated into monthly solutions using GLOBK and combined with 16 North America tracking stations that define the Stable North America Reference Frame (Herring et al., 2008) to derive station position time series using the QOCA software (see Data and Resources). The processes are repeated several times to check and remove outliers. The final monthly solutions are inverted for station positions, velocities, coseismic offsets, and postseismic displacements of large earthquakes through a Kalman filtering procedure used in the QOCA software.

The UCSD Scripps' survey GPS velocities are obtained from González-Ortega et al. (2018). In their data processing, they analyzed survey and CGPS data for northern Baja California during the period from 1993 to 2010 using the GAMIT/GLOBK software package (Herring et al., 2018a). In addition, the SOPAC database, the Salton trough high-resolution interseismic velocity field (Crowell et al., 2013), and the Southern California Earthquake Center (SCEC) Crustal Motion Map version 4 (Shen et al., 2011) were used to inform and complement their data analysis. A total of 64 survey GPS velocities relative to ITRF2008 are collected for their studies.

The NASA JPL and SOPAC velocities are a CGPS velocity product produced by the MEaSUREs project (Bock et al., 2021, see Data and Resources). Their CGPS sites consist mostly of the same stations used for PBO velocity field in the WUS. Similar to the CWU GPS product, their velocities are a precise point-positioning solution obtained using the JPL GIPSY/OASIS software package and use the same processing procedure as that of the GAGE PBO project, allowing for an independent three-component position estimation. They were made available through a GPS and Interferometric Synthetic Aperture Radar data integration project of Shen and Liu (2020). An updated version of the velocity product is available at the MEaSUREs project website (see Data and Resources).
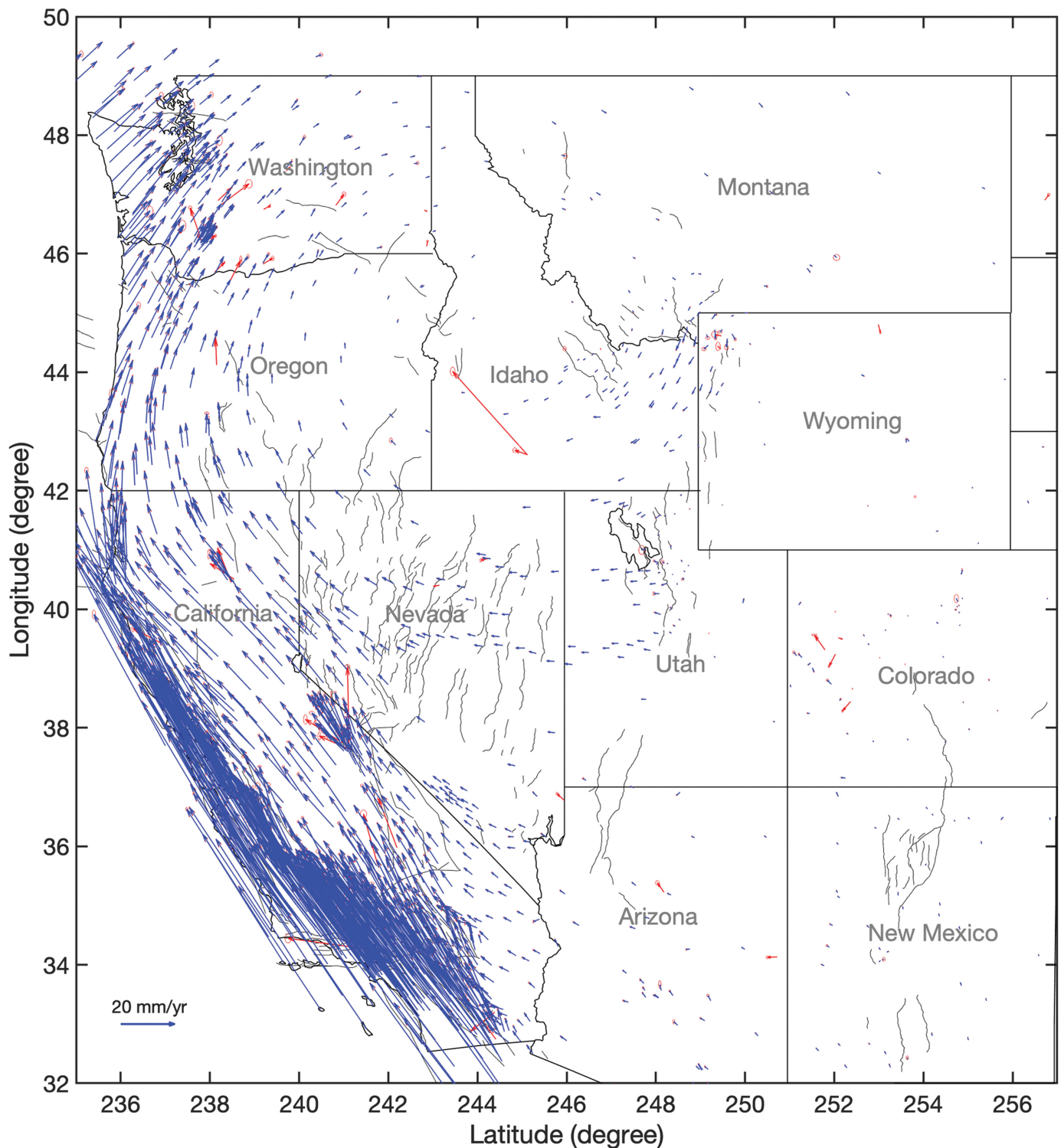
The USGS GPS data consist of both CGPS and survey mode GPS observations across the WUS (Murray and Svarc, 2017). Operated by the geodetic project team at the USGS Earthquake Science Center, survey GPS data have been collected and processed at 1950 sites since 1992 in addition to CGPS operation as part of its earthquake and tectonic research and monitoring program. Both raw survey and continuous data are processed using the GIPSY software package to produce position time series. These positions are aligned to a common North America reference frame and applied through time-series analysis to derive interseismic velocities, coseismic offsets, and poseismic deformation motions. All the USGS GPS velocity products are acquired from the USGS website (see Data and Resources).

Reference Frame, Data Editing, and Combination

All GPS velocity fields reference closely to the North American plate. Their reference frames, however, differ slightly depending on their selections of reference stations. Some adjustments around a few millimeters per year are required to align them exactly with the same average North American plate motion. I choose the PBO North American frame NAM14 (Altamimi et al., 2017) as the target reference frame. All other velocity fields are rotated to this reference frame using a rotation procedure applied in SCEC crustal motion map projects (Shen et al., 2011). For each velocity field, an optimal Euler pole location and its angular rotation parameter is obtained by minimizing the residual velocities between common stations among PBO and the selected velocity field. Based on this optimal Euler pole and angular rotation parameter, I then rotate the velocity field to the PBO North American reference frame. Care is taken to avoid outliers when selecting common stations between the two datasets. This procedure is repeated for the rest of the other six velocity fields. I exclude velocity vectors with uncertainty larger than 2.0 mm/yr from consideration in the frame alignment process and in the final velocity combination.
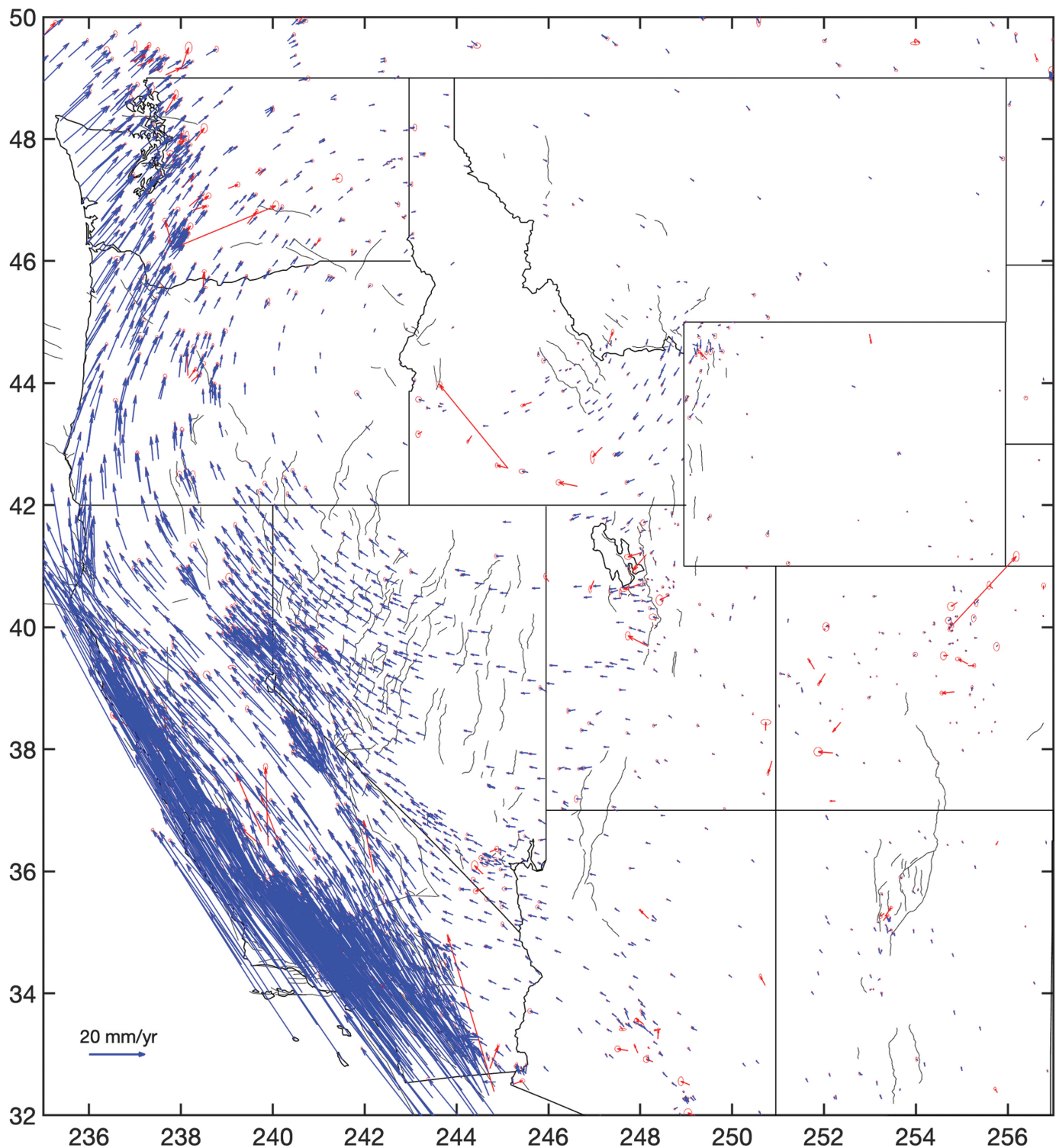
Figures 1–7 show the GPS vectors for all seven rotated velocity fields. For an interseismic velocity field (after correction for any coseismic signals), we would generally expect a spatially smoothly varying velocity. I first edit the velocity fields based on visual inspection. For example, I inspect the velocities for their consistency with neighbors if they are not near faults. In examination of these velocity fields, many obvious data outliers with large variability in amplitude or azimuthal direction are first excluded. For other suspected outliers, I evaluate their differences between neighboring sites. If the differences are over 20% in amplitude or 20° in azimuthal direction or both, I remove them from the dataset. For many of the survey mode GPS velocities, for example, in the UCLA dataset, I compare them with nearby PBO or MIDAS CGPS velocities. I apply the same criterions to remove outliers from these survey mode velocities. For sites near-active volcanic areas, such as Mt. St. Helens, Rainier, Three Sisters, Shasta, and Long Valley caldera, I remove data if they differ significantly from their nonvolcanic neighbors. To avoid any model related biases, deformation model predictions are not applied to discriminate or remove any inconsistent data. Figures 1–7 plot the edited GPS velocity vectors in blue for comparison with the removed velocity outliers in red.

Figure 1. Map of Plate Boundary Observatory (PBO) Global Positioning System (GPS) velocity field for the western United States (WUS) references to the North America Reference Frame NAM14. Red velocity vectors are outliers removed from the solution after rigorous data editing. The color version of this figure is available only in the electronic edition.
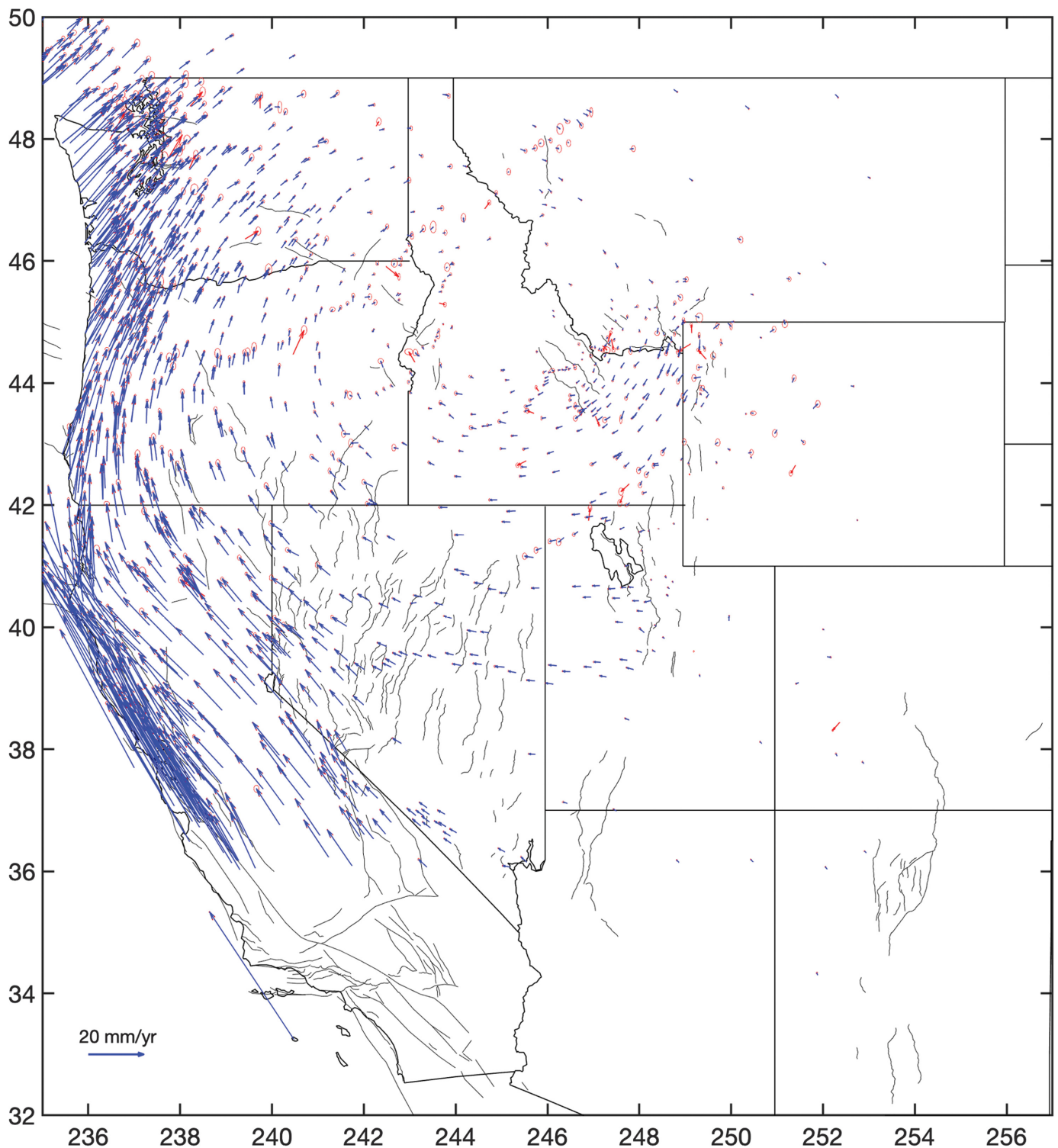
Reported uncertainties in some of the continuous mode velocities are very small, for example, less than 0.1 mm/yr. These velocities could out-weigh other data and bias the least-squares-based inverse solutions. A lower cutoff of uncertainty at 0.2 mm/yr is applied to all velocity fields following Parsons *et al.* (2013). Finally, all seven velocity fields are merged into a single velocity field. In this combined field, a simple arithmetic mean of the components of velocities is

Figure 2. Map of Median Interannual Difference Adjusted for Skewness (MIDAS) (Nevada Geodetic Laboratory [NGL]) GPS velocity field for the WUS references to the North America Reference Frame NAM14. Red velocity vectors are outliers removed from the solution after rigorous data editing. The color version of this figure is available only in the electronic edition.

assigned to a site with multiple velocities. Their uncertainties are calculated as the square root of the sum of their average squared uncertainties and the squared uncertainties due to differences between velocity fields. A total of 4979 horizontal velocity vectors are obtained for the final velocity field.

In comparison to the GPS dataset used for the 2014 NSHM deformation model studies, the number of total data points
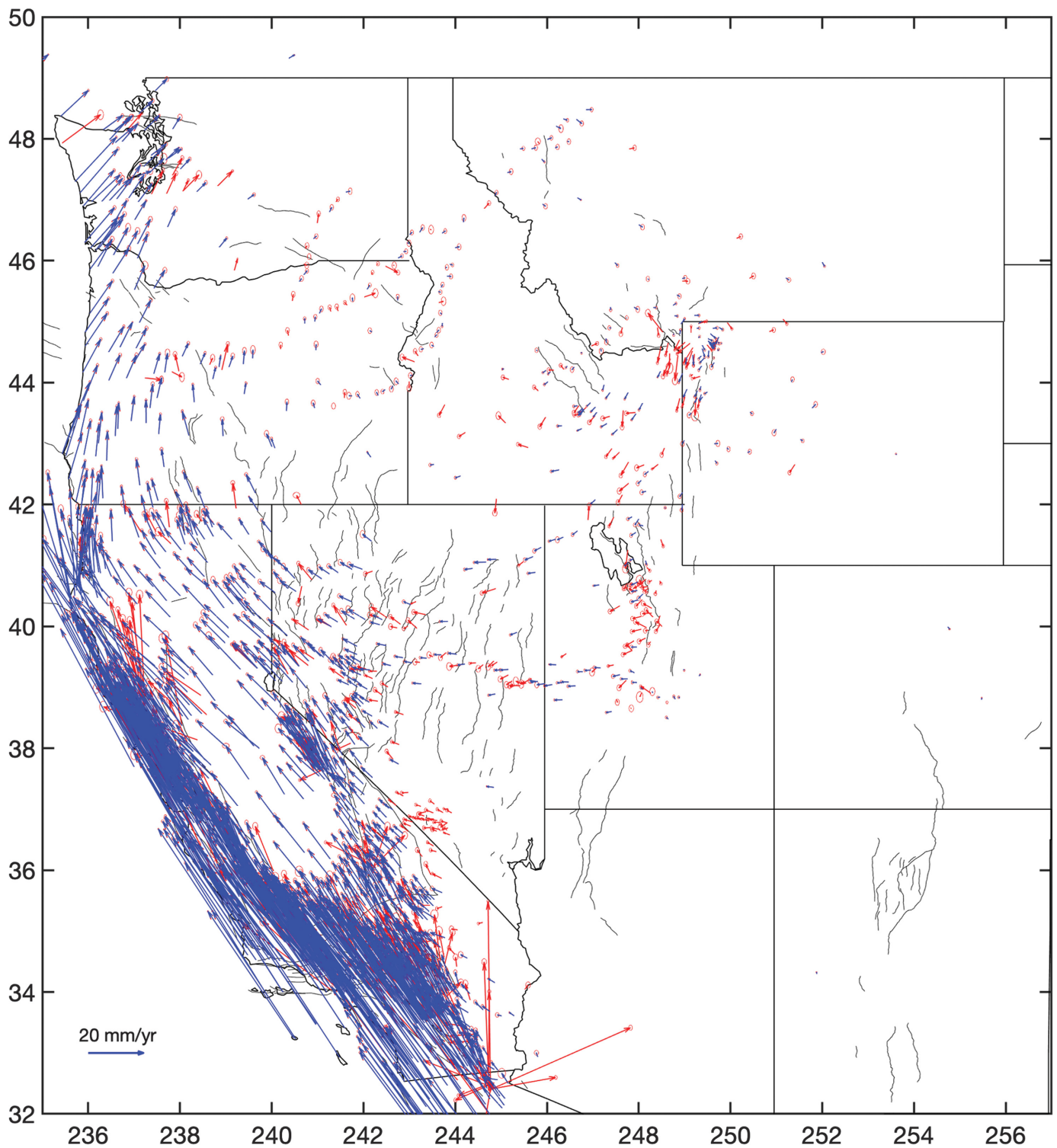
Figure 3. Map of Pacific Northwest GPS velocity field for the WUS references to the North America Reference Frame NAM14. Red velocity vectors are outliers removed from the solution after rigorous data editing. The color version of this figure is available only in the electronic edition.

increased 50%. Figure 8 shows the final velocity field. GPS stations are extremely dense along the San Andreas Fault system. Data coverage is also dense along the Cascadia subduction region across Washington, Oregon, and northern California. Data are also dense along the Walker Lane region and the Intermountain West Seismic Belt. Data coverage is sparse across other WUS area east of the Intermountain West Seismic Belt and around the Front Range.
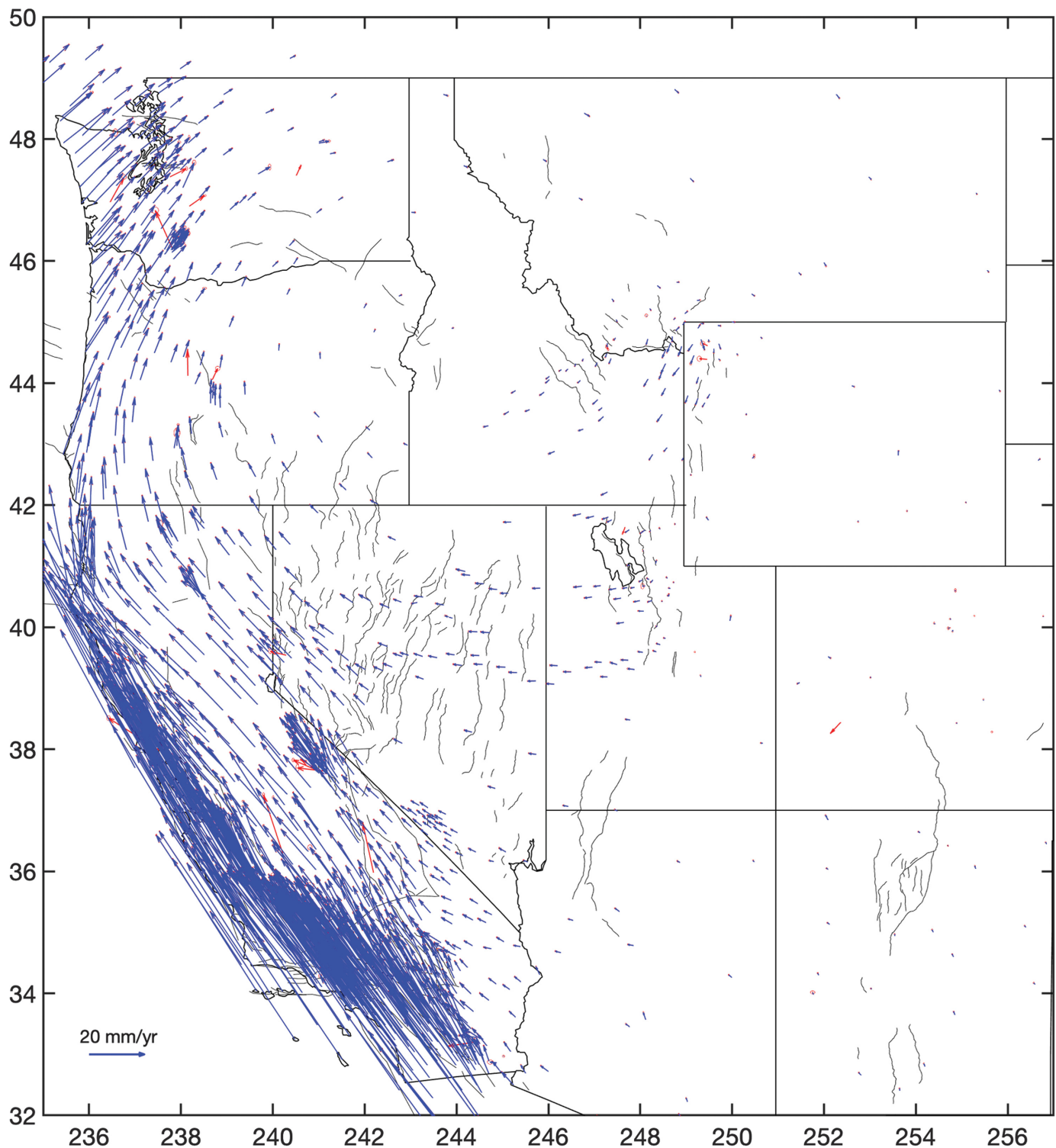
Figure 4. Map of Scripps Institution of Oceanography survey GPS velocity field for the WUS references to the North America Reference Frame NAM14. Red velocity vectors are outliers removed from the solution after rigorous data editing. The color version of this figure is available only in the electronic edition.

GPS Strain Rate

Based on the updated GPS velocities, strain-rate maps for the WUS are developed using the method of Shen *et al.* (2015). Figure 9a,b shows maps of the shear and dilatation strain rates, respectively, across the WUS. With 50% more data coverage than in 2014 in many areas of the WUS, these maps resolve strain accumulation in the actively deforming regions better in terms of spatial resolution than previous strain maps (i.e., Petersen
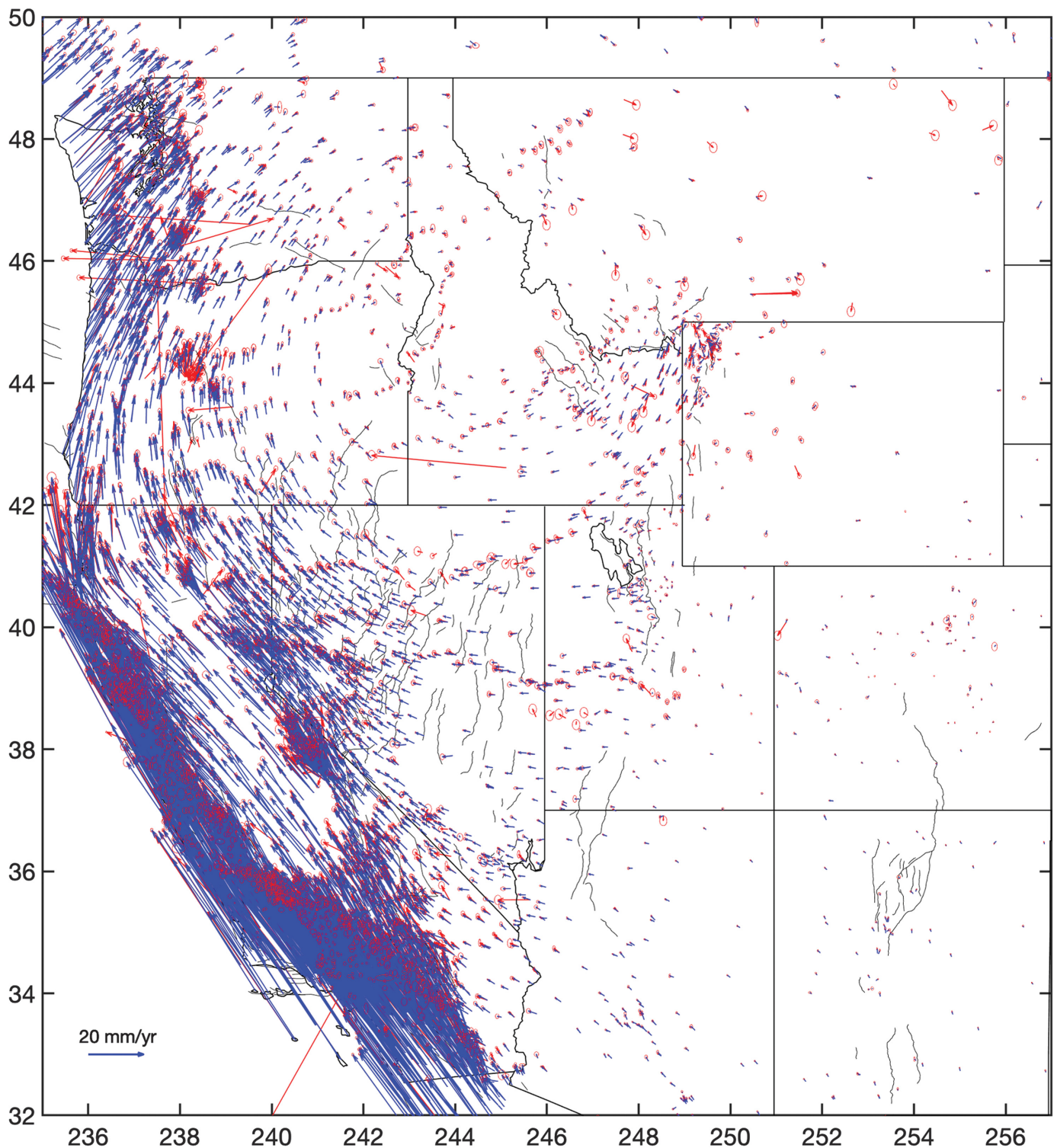
Figure 5. Map of University of California Los Angeles (UCLA) GPS velocity field for the WUS references to the North America Reference Frame NAM14. Red velocity vectors are outliers removed from the solution after rigorous data editing. The color version of this figure is available only in the electronic edition.

et al., 2013). We find highly concentrated shear-strain rate around the San Andreas fault system (Fig. 10b), up to several hundred nanostrain/yr, spanning areas in the south near the northern Baja California to the segments north near the Mendocino Triple Junction. Shear-strain rates are up to 100 nanostrain/yr along the central Nevada seismic belt and Walker Lane, and south to the Garlock and Eastern California Shear zone. High shear-strain rates also appear along the Cascadia
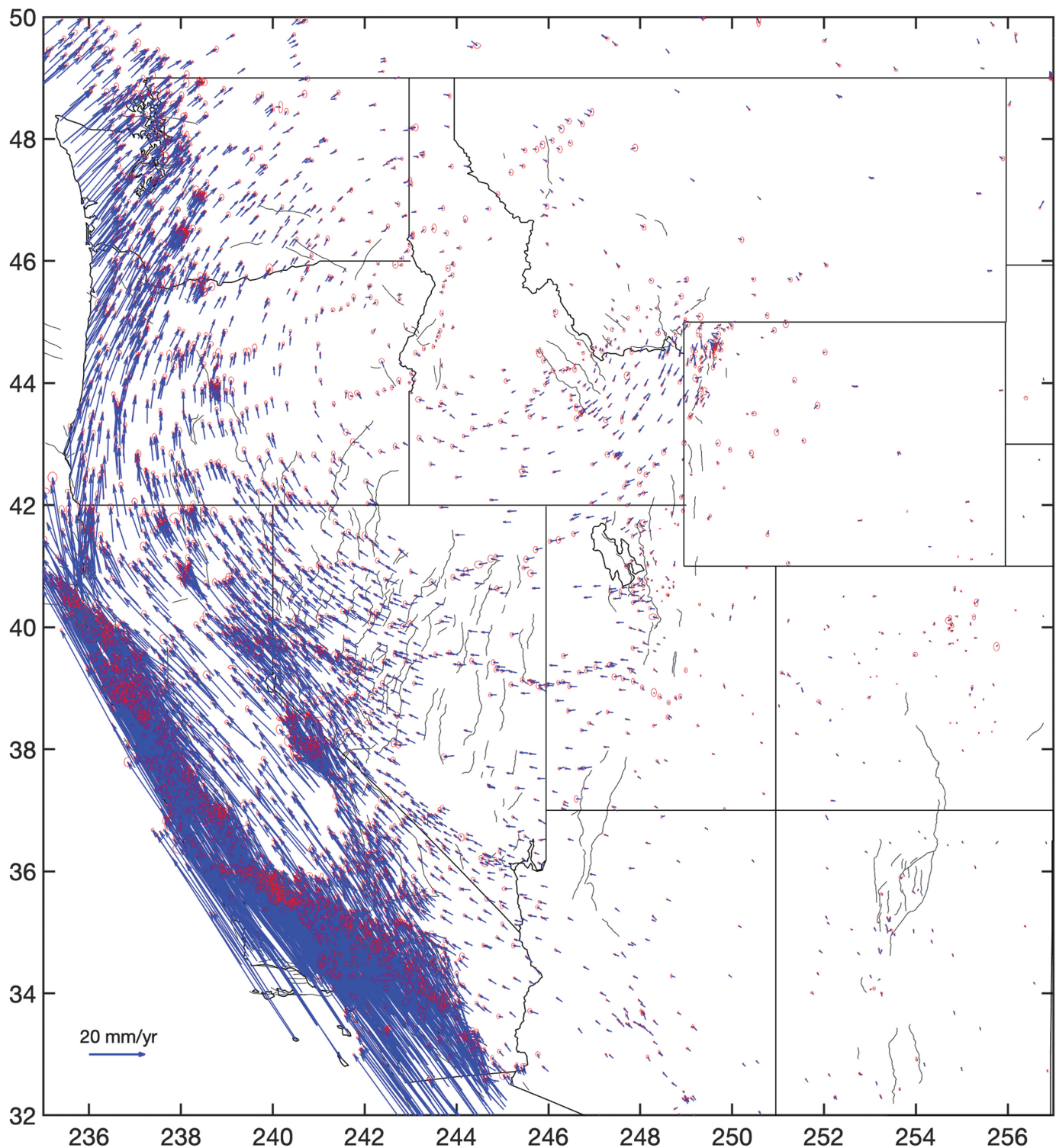
Figure 6. Map Jet Propulsion Laboratory and Scripps Orbit and Permanent Array Center (JPL and SOPAC) GPS velocity field for the WUS references to the North America Reference Frame NAM14. Red velocity vectors are outliers removed from the solution after rigorous data editing. The color version of this figure is available only in the electronic edition.

subduction zone and the Intermountain West Seismic Belt. Some of the high strain rates are caused by volcanism, for example, around Mt. St. Helens, Rainier, Three Sisters, Shasta, and Long Valley caldera. Low strain rates appear across the Sierra Nevada–Great Valley block, indicating a near-rigid behavior of the block. Low strain rates are also found in most parts of the Basin and Range province and the Great Plain east of the Intermountain Seismic Belt.

Figure 7. Map of U.S. Geological Survey (USGS) GPS velocity field for the WUS references to the North America Reference Frame NAM14. Red velocity vectors are outliers removed from the solution after rigorous data editing. The color version of this figure is available only in the electronic edition.

The dilatation rates shown in Figure 9b provide important earthquake faulting information. In the Pacific Northwest, compressional strain rate dominates over shear-strain rate, mostly from the elastic strain caused by the locked subduction zone. Few thrust faults are active in the upper plate, mainly accommodating north–south contraction. In the Intermountain West, extensional strain dominates over shear strain, meaning a higher rate of normal faulting than strike-

Figure 8. Final combined GPS velocity vectors for the WUS region, referenced to the North American plate (NAM14). The color version of this figure is available only in the electronic edition.

slip faulting mechanisms are typical. These results will be useful for geodetic and geologic deformation modeling in support of the 2023 NSHM update.

Figure 10a,b shows maps of the second invariant of the strain rate tensor and seismicity distribution, respectively. In comparison between Figures 10a and 9a, we see very similar pattern of spatial distribution between the second invariant and shear-strain rate. The second invariant of the strain-rate tensor can

be considered a proxy for the maximum strain rate. Compared to seismicity, we find that high strain rates correlate closely with high seismicity rates in the WUS, indicating that earthquakes tend to occur at places where strain rates are
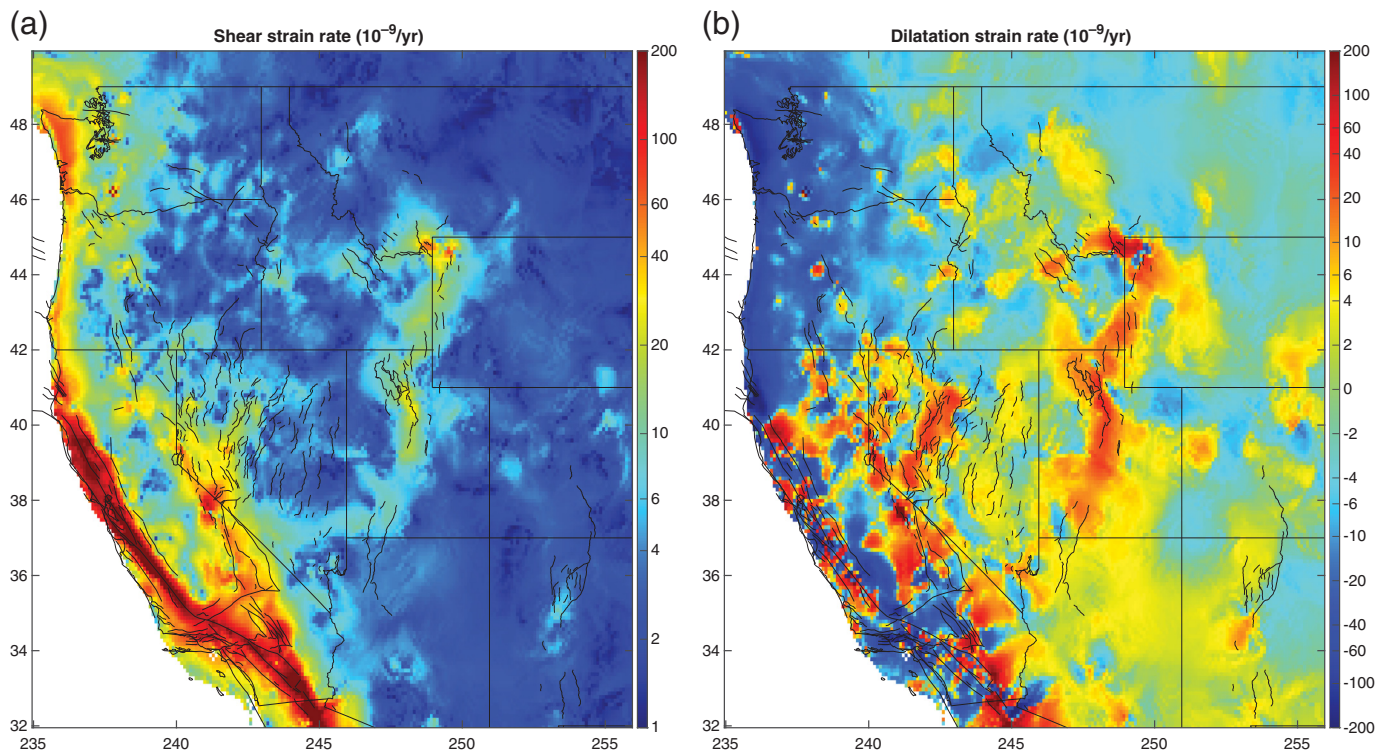
Figure 9. Maps showing distribution of GPS strain-rate distribution in the WUS in nanostrain/year in which (a) shear-strain rate and (b) dilatation-strain rate.
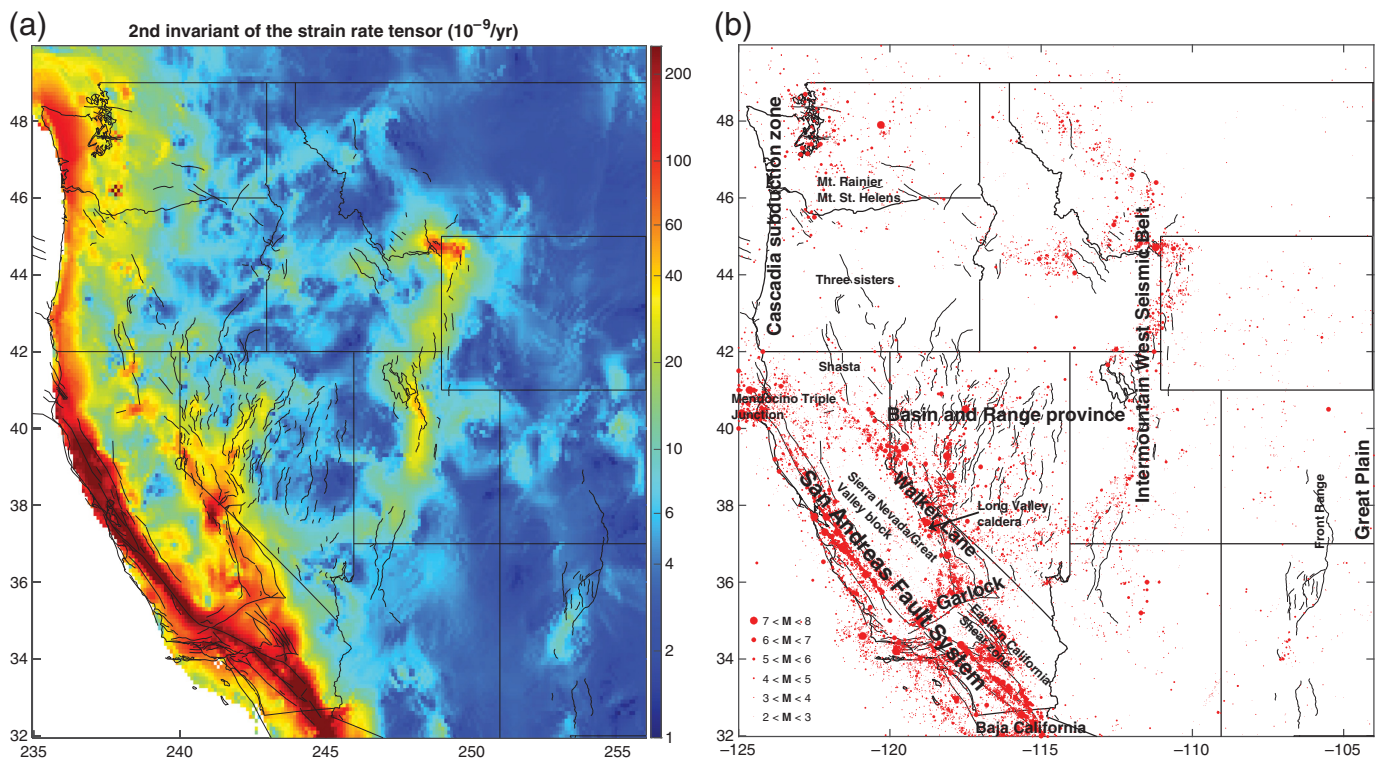
Figure 10. (a) Map view of the second invariant of the strain-rate tensor distribution in the WUS. The unit in the vertical color bar is in nanostrain/year. (b) Map view of the seismicity distribution in the WUS.

higher. For areas of low strain rates, seismic activities are also low.

Conclusions

New WUS GPS velocities solutions are compiled from seven data processing centers for the deformation modeling project in support of the 2023 NSHM update. The solutions include both survey and CGPS velocity products, covering most of the WUS. Following the same processing procedure for UCERF3 and the 2014 NSHM deformation modeling project, I rotate all GPS velocity vectors to a common North American reference frame and edit the fields to remove outliers and velocities with active volcanic deformation. Velocities with uncertainties larger than 2 mm/yr are also removed from the data. The resulting solutions are combined into a final GPS velocity field of 4979 horizontal velocity vectors (Zeng, 2022). GPS station coverage is most dense across California and Nevada. Regions along the Cascadia subduction area and the Intermountain West Seismic Belt are also well covered by the GPS stations. I compute strain rates using these GPS velocities by applying the method of Shen *et al.* (2015). We find high strain rate across the San Andreas fault system, and along the Walker Lane and Eastern California Shear zone. High strain rates also appear along coastal regions of Washington and Oregon associated with the Cascadia Subduction Zone, and regions across the Intermountain West Seismic Belt. These strain rates correlate well with seismicity rates, indicating increasing rates of earthquakes where strain rates are high. The final GPS velocity field is applied for geodetic and geologic deformation modeling in the WUS.

Data and Resources

The Plate Boundary Observatory (PBO) Global Positioning System (GPS) velocity product is available from the UNAVCO data center at https://data.unavco.org/archive/gnss/products/velocity/ (last accessed May 2022). These data were released on 9 July 2019 and is the last version of the Geodesy Advancing Geosciences and EarthScope (GAGE) PBO product. The Median Interannual Difference Adjusted for Skewness (MIDAS) GPS velocities are available from the Nevada Geodetic Laboratory (NGL) data archives at its website http://geodesy.unr.edu/ (last accessed March 2020). The U.S. Geological Survey (USGS) velocity data are available at https://earthquake.usgs.gov/monitoring/gps (last accessed May 2022). The Pacific Northwest GPS field data are archived at the UNAVCO data center and the processed time series and velocities are available upon request from Robert McCaffery (Portland State University [PSU], written comm., 2020). The University of California Los Angeles (UCLA) data are from an unpublished work of Zheng-Kang Shen (UCLA, written comm., 2020). The Scripps Orbit and Permanent Array Center (SOPAC) data are available at http://sopac.ucsd.edu (last accessed March 2020). The Jet Propulsion Laboratory/Scripps Orbit and Permanent Array Center (JPL/SOPAC) velocities are from their MEaSUREs project available at http://garner.ucsd.edu/pub/measuresESESES_products/ (username: anonymous; password: your e-mail address) (last accessed August 2022). The QOCA software

is from JPL website at https://qoca.jpl.nasa.gov/ (last accessed August 2022). The final GPS velocity field of this study is available in the supplemental material of this article or Zeng (2022).

Declaration of Competing Interests

The author acknowledges that there are no conflicts of interest recorded.

References

Altamimi, Z., L. Métivier, P. Rebischung, H. Rouby, and X. Collilieux (2017). ITRF2014 plate motion model, *Geophys. J. Int.* **209,** no. 3, 1906–1912, doi: 10.1093/gji/ggx136.

Argus, D. F., Y. Fu, and F. W. Landerer (2014). Seasonal variation in total water storage in California inferred from GPS observations of vertical land motion, *Geophys. Res. Lett.* **41,** 1971–1980, doi: 10.1002/2014GL059570.

Blewitt, G., W. C. Hammond, and C. Kreemer (2018). Harnessing the GPS data explosion for interdisciplinary science, *Eos* **99,** doi: 10.1029/2018EO104623.

Blewitt, G., C. Kreemer, W. C. Hammond, and J. Gazeaux (2016). MIDAS robust trend estimator for accurate GPS station velocities without step detection, *J. Geophys. Res.* **121,** doi: 10.1002/2015JB012552.

Bock, Y., A. W. Moore, D. Argus, P. Fang, D. Golriz, K. Guns, S. Jiang, S. Kedar, S. A. Knox, Z. Liu, *et al.* (2021). Extended Solid Earth Science ESDR System (ES3): Algorithm Theoretical Basis Document, NASA MEaSUREs project, #NNH17ZDA001N, available at http://garner.ucsd.edu/pub/measuresESESES_products/ATBD/ESESES-ATBD.pdf (username: anonymous; password - your e-mail address) (last accessed August 2022).

Crowell, B. W., Y. Bock, D. T. Sandwell, and Y. Fialko (2013). Geodetic investigation into the deformation of the Salton trough, *J. Geophys. Res.* **118,** no. 9, 5030–5039, doi: 10.1002/jgrb.50347.

González-Ortega, J. A., J. J. González-García, and D. T. Sandwell (2018). Interseismic velocity field and seismic moment release in northern Baja California, Mexico, *Seismol. Res. Lett.* **89,** no. 2A, doi: 10.1785/0220170133.

Hammond, W. C., R. Burgette, K. Johnson, and G. Blewitt (2018). Uplift of the Western Transverse Ranges and Ventura area of Southern California: A four-technique geodetic study combining GPS, InSAR, leveling and tide gauges, *J. Geophys. Res.* **122,** 836–858, doi: 10.1002/2017JB014499.

Herring, T., M. Craymer, G. Sella, R. Snay, G. Blewitt, D. Argus, Y. Bock, E. Calais, J. Davis, and M. Tamisiea (2008). SNARF 2.0: A Regional Reference Frame for North America, *Eos Transactions,*

AGU, **89**, no. 23, Joint Assembly Supplement, Abstract G31B-01.

Herring, T. A., M. A. Floyd, R. W. King, and S. C. McClusky (2015). GLOBK Reference Manual, Release 10.6, Massachusetts Institute of Technology, 95 pp., available at https://geoweb.mit.edu/gg/docs/GLOBK_Ref.pdf (last accessed August 2022).

Herring, T. A., R. W. King, M. A. Floyd, and S. C. McClusky (2018a). Introduction to GAMIT/GLOBK, Release 10.7, Massachusetts Institute of Technology, 54 pp., available at https://geoweb.mit.edu/gg/docs/Intro_GG.pdf (last accessed August 2022).

Herring, T. A., R. W. King, M. A. Floyd, and S. C. McClusky (2018b). GAMIT Reference Manual, Release 10.7, Massachusetts Institute of Technology, 168 pp., available at https://geoweb.mit.edu/gg/docs/GAMIT_Ref.pdf (last accessed August 2022).

Herring, T. A., T. I. Melbourne, M. H. Murray, M. A. Floyd, W. M. Szeliga, R. W. King, D. A. Phillips, C. M. Puskas, M. Santillan, and L. Wang (2016). Plate Boundary Observatory and related networks: GPS data analysis methods and geodetic products, *Rev. Geophys.* **54**, doi: 10.1002/2016RG000529.

McCaffrey, R., and R. W. King (2017). Puget 2016, The GAGE Facility operated by UNAVCO, Inc., *GPS/GNSS Observations Dataset*, doi: 10.7283/T5ZK5F30.

McCaffrey, R., P. Bird, J. Bormann, K. M. Haller, W. C. Hammond, W. R. Thatcher, R. E. Wells, Y. Zeng (2013). NSHMP block model of Western United States active tectonics, Appendix A, in *Geodesy- and Geology-Based Slip-Rate Models for the Western United States (excluding California) National Seismic Hazard Maps*, M. D. Petersen *et al.* (Editors), *U.S. Geol. Surv. Open-File Rept. 2013-1293*, 27–38, doi: 10.3133/ofr20131293.

McCaffrey, R., R. W. King, S. J. Payne, and M. Lancaster (2013). Active tectonics of northwestern U.S. inferred from GPS-derived surface velocities, *J. Geophys. Res.* **118**, doi: 10.1029/2012JB009473.

McCaffrey, R., A. I. Qamar, R. W. King, R. Wells, G. Khazaradze, C. A. Williams, C. W. Stevens, J. J. Vollick, and P. C. Zwick (2007). Fault locking, block rotation and crustal deformation in the Pacific Northwest, *Geophys. J. Int.* **169**, 1315–1340, doi: 10.1111/j.1365-246X.2007.03371.x.

Murray, J. R., and J. Svarc (2017). Global positioning system data collection, processing, and analysis conducted by the U.S. Geological Survey Earthquake Hazards Program, *Seismol. Res. Lett.* **88**, no. 3, 916–925.

Parsons, T., M. Johnson, P. Bird, J. Bormann, T. Dawson, E. Field, W. Hammond, T. Herring, R. McCaffrey, Z.-K. Shen, *et al.* (2013). Appendix C—Deformation models for UCERF3, *U.S. Geol. Surv. Open-File Rept. 2013-1165*, 97 pp., doi: 10.3133/ofr20131165.

Petersen, M. D., M. P. Moschetti, P. M. Powers, C. S. Mueller, K. M. Haller, A. D. Frankel, Y. Zeng, S. Rezaeian, S. C. Harmsen, O. S. Boyd, *et al.* (2014). Documentation for the 2014 update of the United States national seismic hazard maps, *U.S. Geol. Surv. Open-File Rept. 2014-1091*, 243 pp., doi: 10.3133/ofr20141091.

Petersen, M. D., Y. Zeng, K. M. Haller, R. McCaffrey, W. C. Hammond, P. Bird, M. P. Moschetti, Z.-K. Shen, J. Bormann, and W. R. Thatcher (2013). Geodesy- and geology-based slip-rate models for the Western United States (excluding California) national seismic hazard maps, *U.S. Geol. Surv. Open-File Rept. 2013-1293*, 80 pp., doi: 10.3133/ofr20131293.

Shen, Z.-K. (2017). Updating Western US Crustal Motion Map, *Final Technical Report of the USGS Earthquake Hazards Program Assistance Awards*, available at https://earthquake.usgs.gov/cfusion/external_grants/reports/G16AP00059.pdf (last accessed August 2022).

Shen, Z.-K., and Z. Liu (2020). Integration of GPS and InSAR data for resolving 3-dimensional crustal deformation, *Earth Space Sci.* **7**, no. 4, doi: 10.1029/2019ea001036.

Shen, Z.-K., R. W. King, D. C. Agnew, M. Wang, T. A. Herring, D. Dong, and P. Fang (2011). A unified analysis of crustal motion in southern California, 1970-2004: The SCEC crustal motion map, *J. Geophys. Res.* **116**, no. B11, doi: 10.2019/2011JB008549.

Shen, Z.-K., M. Wang, Y. Zeng, and F. Wang (2015). Optimal interpolation of spatially discretized geodetic data, *Bull. Seismol. Soc. Am.* **105**, 2117–2127, doi: 10.1785/0120140247.

Zeng, Y. (2022). 2023 NSHM western United States GPS velocities, *U.S. Geol. Surv. Data Release*, doi: 10.5066/P9MXY6RC.

Zeng, Y., and Z.-K. Shen (2013). A fault-based model for crustal deformation in the Western United States, Appendix D, in *Geodesy- and Geology-Based Slip-Rate Models for the Western United States (Excluding California) National Seismic Hazard Maps*, M. D. Petersen *et al.* (Editors), *U.S. Geol. Surv. Open-File Rept. 2013-1293*, 58–68, doi: 10.3133/ofr20131293.